HAL
open science

# Research on Efficient Fast Scintillators: Evidence and X-Ray Absorption Near Edge Spectroscopy Characterization of Ce 4+ in Ce 3+ , Mg 2+ -Co-Doped Gd 3 Al 2 Ga 3 O 12 Garnet Crystal

Géraldine Dantelle, Georges Boulon, Yannick Guyot, Denis Testemale, Malgorzata Guzik, Shunsuke Kurosawa, Kei Kamada, Akira Yoshikawa

## To cite this version:

Géraldine Dantelle, Georges Boulon, Yannick Guyot, Denis Testemale, Malgorzata Guzik, et al.. Research on Efficient Fast Scintillators: Evidence and X-Ray Absorption Near Edge Spectroscopy Characterization of Ce 4+ in Ce 3+ , Mg 2+ -Co-Doped Gd 3 Al 2 Ga 3 O 12 Garnet Crystal. physica status solidi (b), 2020, 257 (8), pp.1900510. 10.1002/pssb.201900510 . hal-02508822

**HAL Id: hal-02508822**

**https://hal.science/hal-02508822v1**

Submitted on 3 Nov 2020

**HAL** is a multi-disciplinary open access archive for the deposit and dissemination of scientific research documents, whether they are published or not. The documents may come from teaching and research institutions in France or abroad, or from public or private research centers.

L'archive ouverte pluridisciplinaire **HAL**, est destinée au dépôt et à la diffusion de documents scientifiques de niveau recherche, publiés ou non, émanant des établissements d'enseignement et de recherche français ou étrangers, des laboratoires publics ou privés.

# Research of efficient fast scintillators. Evidence and XANES characterization of $Ce^{4+}$ in $Ce^{3+}$, $Mg^{2+}$-co-doped $Gd_3Al_2Ga_3O_{12}$ garnet crystals

*Géraldine Dantelle, Georges Boulon*, Yannick Guyot, Denis Testemale, Malgorzata Guzik, Shunsuke Kurosawa, Kei Kamada, Akira Yoshikawa*

Dr. Géraldine Dantelle, Dr. Denis Testemale
Institut NEEL, CNRS/UGA UPR2940, 25 rue des Martyrs Grenoble, France and
ESRF, European Synchrotron Radiation Facility, 38042 Grenoble, France

Prof. Georges Boulon, Assoc. Prof. Yannick Guyot
Institut Lumière Matière (ILM), UMR5306 CNRS-UCB Lyon1, Université de Lyon, 69622 Villeurbanne, France
*georges.boulon@univ-lyon1.fr

Assoc. Prof. Malgorzata Guzik
Faculty of Chemistry, University of Wroclaw, ul. Joliot-Curie 14, 50-383 Wroclaw, Poland

Assoc. Prof. Shunsuke Kurosawa, Assoc. Prof. Kei Kamada, Prof. Akira Yoshikawa
Institute for Material Reseach (IMR), Tohoku University, 2-1-1 Katahira Aoba-ku, Sendai, 980-8577 Miyagi, Japan

**Keywords :** fast scintillator, $Ce^{3+}$ and $Ce^{4+}$ dopants, garnet crystals, optical spectroscopy, XANES spectroscopy

**Abstract**

In this paper, the most advanced oxide scintillator $Ce^{3+}$, $Mg^{2+}$-co-doped $Gd_3Al_2Ga_3O_{12}$ (GAGG) garnet host, grown by using the Czochralski method at the Tohoku University, Sendai, is reported. The charge transfer absorption band in UV, like in other $Ce^{3+}$, $Mg^{2+}$-co-doped oxides, reveals the creation of stable $Ce^{4+}$ oxidation state, in addition of the usual $Ce^{3+}$ one, admitted as responsible of the scintillation mechanism improvement displayed by this garnet. Strangely, the confirmation of quantitative values of $Ce^{4+}$ concentration has never been done and the goal is mainly focused on the presence of $Ce^{4+}$ and the evaluation of the $Ce^{3+}/Ce^{4+}$ ratio measured by XANES spectroscopy at the Ce $L_{III}$ threshold of the European Synchrotron Radiation Facility (ESRF). This result is compared with those obtained for $Ce^{3+}$, $Mg^{2+}$-co-doped LuAG and, also, in garnets without any $Mg^{2+}$ions like $Ce^{3+}$-doped GAGG,

This article has been accepted for publication and undergone full peer review but has not been through the copyediting, typesetting, pagination and proofreading process, which may lead to differences between this version and the Version of Record. Please cite this article as doi: 10.1002/pssb.201900510

This article is protected by copyright. All rights reserved

Accepted Article

$Ce^{3+}$-doped LuAG and $Ce^{3+}$-doped YAG. The role of $Li^{+}$ ion in place of $Mg^{2+}$ one is also considered in $Ce^{3+}$, $Li^{+}$-co-doped LuAG single crystal.

## 1. Introduction: state of the art of research on new fast garnet scintillators

Research on new fast inorganic scintillation crystals, is a critical pillar in the strategy of PET, a nuclear medicine imaging technique.[1-3] Actually, the best scintillators used to convert high-energy radiation of the two gamma rays to UV-visible radiation are based of $Ce^{3+}$ dopant in crystals, due to the parity-allowed electric dipole 5d-4f transitions which have larger oscillator strengths and shorter radiative lifetimes than the 4f-4f transitions of the trivalent rare earth ions. Selected scintillator crystals were $Ce^{3+}$-doped orthosilicates as $Gd_2SiO_5$ (GSO), $Lu_2SiO_5$ (LSO), $(Lu_{1-x}Y_x)_2SiO_5$ (LYSO).[4-7] As we always have to improve spatial and temporal performances of these scintillator crystals, great efforts are made to find new compounds like pyrosilicates based on $RE_2Si_2O_7$ (RE = Lu, Y,Gd), $LaX_3$ (X = Cl, Br) single crystal hosts. [8-10] Also very important is research on garnet structure single crystals which are indeed promising candidates by combining high values of both density, stopping power for X-ray and γ-ray radiations and light yield. Well mastered crystal growth technology is deeply developed for doping by rare earth ions like $Pr^{3+}$, $Nd^{3+}$, $Ho^{3+}$, $Er^{3+}$, $Tm^{3+}$, $Yb^{3+}$ for lasers sources, $Ce^{3+}$ for phosphors or $Tb^{3+}$ for magneto-optic hosts. A remarkable scintillator-oriented combinatorial search in $Ce^{3+}$-doped $(Y,Gd)_3(Ga,Al)_5O_{12}$ multi-component garnet compounds leads to find out new $Ce^{3+}$-doped $Gd_3Al_2Ga_3O_{12}$ (GAGG) single crystals which have been demontrated to be efficient exceeding the light yield values achieved for the best commercially used $Ce^{3+}$-doped LYSO orthosilicate crystals.[11-24] The research was also extended by $Ce^{3+}$-doped garnet transparent ceramics of similar garnet compositions to single crystals which have displayed a more intense and faster scintillation signal than crystals.[25-27]

## 2. Role of $Ce^{4+}$ cations in the scintillation mechanism

In order to improve the time response properties and the light yield of several types of scintillators an approach has been made by codoping with divalent alkali earth elements such as $Ca^{2+}$ and $Mg^{2+}$ ions, changing the $Ce^{3+}$ valence state into the $Ce^{4+}$ one by the charge compensation mechanism which achieves charge neutrality.[14, 18, 20, 21]

Accepted Article

This article is protected by copyright. All rights reserved

The presence of $Ce^{4+}$ ions in $Ce^{3+}$-doped materials has always been a big issue. The first precise work showing the presence of $Ce^{4+}$ has been published in 1992 by Rotmann on $Ce^{3+}$, $Ca^{2+}$-co-doped YAG.[28] Optically, it has been determined that the cerium can change valence state between $Ce^{3+}$ and $Ce^{4+}$ when annealed in an atmosphere of reducing and oxidizing gases, respectively. Under cathodoluminescence, the $Ce^{3+}$ ion emission is seen even when only $Ce^{4+}$ is present in the crystal and it was interpreted as an electron first entering a $Ce^{4+}$ in an upper excited 5d state, thereby converting it temporarily to $Ce^{3+}$, followed by the standard 5d→4f emission of $Ce^{3+}$ at 550 nm. Then, in 2013, Blahuta & al. proposed, a new scintillation mechanism under ionizing irradiation involving $Ce^{4+}$ ions in $Ce^{3+}$-$Mg^{2+}$/$Ca^{2+}$-co-doped LYSO single crystals.[7] Nowadays, in co-doped materials, the evidence of $Ce^{4+}$ is admitted for the sequential charge capture of an electron-hole pair by $Ce^{3+}$ according to:

$$Ce^{3+} + e^{-} + h^{+} \rightarrow Ce^{4+} + e^{-} \rightarrow (Ce^{3+})^{*} \rightarrow Ce^{3+} + h\nu$$

Then, there is a continuous process of capturing a hole from the valency band.

As a result, $Ce^{4+}$ ions are stabilized by the addition of $Mg^{2+}$/$Ca^{2+}$ divalent ions.[14,18, 20, 21] Such centers create another fast radiative recombination pathway working in parallel with the classical mechanism based on the stable $Ce^{3+}$ centers. It means the skipping of the first hole trapping stage could result in acceleration of the decay by suppression of slow components.[29]

This observation has to be combined with the favorable position of the shallow levels below the conduction band leading to slow components of the decay. The main purpose of the $Mg^{2+}$/$Ca^{2+}$-co-dopant as analyzed by Melcher's group was to limit the formation of vacancies (Vo) that were detrimental in term of afterglow level.[14,18 ] All previous results on $Ce^{3+}$, $Mg^{2+}$-co-doped GAGG are in favour of a promising scintillator for timing devices in high-energy physics and Time-of-Flight PET (TOF-PET) applications.

In this way, in the following part, we summarize the main spectroscopic properties of $Ce^{3+}$-doped GAGG and $Ce^{3+}$, $Mg^{2+}$-co-doped GAGG garnet crystals.

## 3. Crystal growth and spectroscopic properties of $Ce^{3+}$-doped $Gd_3Al_2Ga_3O_{12}$ (GAGG) and $Ce^{3+}$, $Mg^{2+}$-co-doped GAGG garnet crystals

Especially, the $Ce^{3+}$-doped GAGG shown in **Figure 1a** and the $Ce^{3+}$, $Mg^{2+}$-co-doped GAGG shown in **Figure 1b** are single crystals developed by using the Czochralski method at IMR, Tohoku University.[15, 21]

The absorption spectra of 0.5% $Ce^{3+}$-doped GAGG and 0.5% $Ce^{3+}$, 0.5% $Mg^{2+}$-co-doped GAGG crystals are presented in **Figure 2**. We clearly see the two first $Ce^{3+}$ 4f→5d absorption

This article is protected by copyright. All rights reserved

bands at roughly 450 and 340 nm, respectively, the $Gd^{3+}$ 4f $^8S_{7/2} \rightarrow {}^6P_J$ and $^8S_{7/2} \rightarrow {}^6I_J$ absorption lines and, especially in the co-doped crystal, the strong $Ce^{4+}$ charge transfer band (CTB) in UV below 320 nm. This CTB is assigned from the oxygen 2p orbitals of the valence band to the $Ce^{4+}$ 4f orbitals by analogy with $Ce^{3+}$,$Mg^{2+}$/$Ca^{2+}$-co-doped LYSO[7] and also with $Ce^{3+}$, $Mg^{2+}$-co-doped $Lu_3Al_5O_{12}$ (LuAG) ceramics.[26] The hole in the maximum of this broad absorption band at around 275 nm corresponds to the resonant energy transfer between the $Gd^{3+}$ $^6I_J \rightarrow {}^8S_{7/2}$ emission lines and the $Ce^{4+}$ CTB broad absorption which corresponds to a non-radiative energy transfer since $Ce^{4+}$ centers do not emit. Finally, in $Ce^{3+}$, $Mg^{2+}$-co-doped GAGG there is two contributions to shortening of the decay: one due to the presence of $Ce^{4+}$ and another one associated with the energy transfer from $Gd^{3+}$ to $Ce^{4+}$ ions. A discussion on the energy migration and energy transfer processes in the set of un-doped and $Ce^{3+}$ activated multi-component garnet single crystals has ben recently reported.[30]

Radioluminescence spectra under excitation by X-rays from CuKa of the $Ce^{3+}$-doped GAGG and $Ce^{3+}$, $Mg^{2+}$ co-doped GAGG are shown in **Figure 3**. The broad visible band is composed of the two usual transitions 5d→4f ($^2F_{5/2}$) and 5d→4f ($^2F_{7/2}$). It is important to mention the decreasing of the $Ce^{3+}$ emission intensity by $Mg^{2+}$ co-doping as a result of the creation of $Ce^{4+}$ in these crystals and then the reduction of $Ce^{3+}$ active centers.

Scintillation decays of the 5d→4f visible broad band of 1% $Ce^{3+}$-doped GAGG (0% Mg) and 1% $Ce^{3+}$,0.1% $Mg^{2+}$ co-doped GAGG crystals under excitation by $^{137}Cs$ radio-isotope (662 keV) are shown in **Figure 4**. Decay profiles can be fitted by two exponentials, corresponding to the fast and slow radiative recombination of the $Ce^{3+}$ emitting centers. The decay-time components of 1% $Ce^{3+}$-doped GAGG (0% Mg) and 1% $Ce^{3+}$,0.1% $Mg^{2+}$ co-doped GAGG crystals and the corresponding percentage of the total scintillation output are listed in **Table 1**. The most prominent observation is the shortening of the scintillation decay-time after $Mg^{2+}$ co-doping. Without $Mg^{2+}$,1% $Ce^{3+}$-doped GAGG is characterized by 92.2 ns decay time (81%) and in 1% $Ce^{3+}$, 0.1% $Mg^{2+}$ co-doped GAGG 58% of the total decay by 45.2 ns decay time. The shortening was already noticed first in $Ce^{3+}$, $Mg^{2+}$/$Ca^{2+}$-co-doped LYSO crystal[7], in $Ce^{3+}$, $Ca^{2+}$-co-doped GAGG crystal[14] and $Ce^{3+}$, $Mg^{2+}$-co-doped LuAG ceramics.[25-27]

Accepted Article

This article is protected by copyright. All rights reserved

**Table 1** The decay-time components of 1% $Ce^{3+}$-doped GAGG (0% Mg) and 1% $Ce^{3+}$, 0.1% $Mg^{2+}$ co-doped GAGG crystals and the corresponding percentage of the total scintillation output.

| Samples | Light output % | Fast decay time (ns)/ ratio (%) | Slow decay time (ns)/ ratio (%) | Timing resolution/ps |
|---|---|---|---|---|
| 0 % Mg | 100 | 92.2/81 | 296/19 | 452 |
| 0.1% Mg (1000 at.ppm) | 79 | 45.2/58 | 135/42 | 196 |
| 0.01% Mg (100 at.ppm) | 93.5 | 39.6/53 | 132/47 | |

In $Ce^{3+}$-doped $Gd_3Al_2Ga_3O_{12}$ single crystals, we should add the scintillation decays were accelerated by both $Ca^{2+}$ and $Mg^{2+}$ co-dopants. Comparing to $Ca^{2+}$ co-doping, the $Mg^{2+}$ co-doped samples showed much faster decay and comparatively smaller light output decrease with increasing $Mg^{2+}$ dopant concentration but of enough intensity to be applied. The best sample corresponds to 100 at. ppm $Mg^{2+}$ with performances mentioned in **Table1**.

Finally, $Ce^{3+}$, $Mg^{2+}$-co-doped GAGG shows improvement of both, shortening of the decay –time (45.2 ns on 58% of the decay), a fast timing resolution (196 ps, close to 180 ps, the value of the LYSO crystal) and a high light yield (44000 photon/MeV), corresponding to only 79% of the $Ce^{3+}$-doped $Gd_3Al_2Ga_3O_{12}$ light output, so that is really a promising scintillator for application as positron emission tomography.

## 4. Evidence and evaluation of stable $Ce^{4+}$ ions by XANES technique in $Ce^{3+}$, $Mg^{2+}$-co-doped GAGG

Previous articles considered that the charge transfer absorption band located at 260 nm is the probe of presence of $Ce^{4+}$ ions in $Ce^{3+}$, $Mg^{2+}/Ca^{2+}$-co-doped LYSO single crystals[7] and $Ce^{3+}$, $Ca^{2+}$-co-doped GAGG[6, 21]. This hypothesis seems in agreement with the creation of $Ce^{4+}$ ions due to the introduction of divalent ions as $Ca^{2+}$ and $Mg^{2+}$. However, the quantitative values of the $Ce^{3+}/Ce^{4+}$ concentration ratio in $Ce^{3+}$, $Mg^{2+}$-co-doped GAGG have never been measured. Therefore, our goal is firstly focused on the confirmation of the

Accepted Article

This article is protected by copyright. All rights reserved

presence of $Ce^{4+}$ ions in this crystal and secondly on the evaluation of the $Ce^{3+}/Ce^{4+}$ ratio measured by the X-ray Absorption Near Edge Spectroscopy (XANES) spectroscopy at the Ce $L_{III}$ threshold which is another effective technique able to distinguish unambiguously the $Ce^{3+}$ and $Ce^{4+}$ oxidation states. Measurements have been made at the European Synchrotron Radiation Facility (ESRF) in Grenoble performed in high energy resolution fluorescence-detected (HERFD) mode at the Fame-UHD beamline. The photon energy was scanned from 5.68 keV to 5.85 keV using a Si (220) double-crystal monochromator. A glove box filled with helium was used between the samples, the crystal analyzer spectrometer and the detector, to avoid partial beam absorption by the air. The signal was recorded with a five-Ge (331) crystal analyzer and a Vortex-Ex detector. The beam size was 300 x 100 $\mu m^2$ (horizontal x vertical FWHM). The energy calibration was done using the $CeO_2$ spectrum. The $Ce^{3+}/Ce^{4+}$ ratio was determined by linear combination of XANES spectra of standards, *i.e.* nano-$CeO_2$ as a reference for $Ce^{4+}$ and another $Ce^{3+}$-doped YAG single-crystal as a reference for $Ce^{3+}$ [31]. The experimental data were analyzed using the *Demeter/Athena* software.[32] We also have evaluated the $Ce^{3+}/Ce^{4+}$ ratio by withdrawing ratio dependence of XANES spectra corresponding to different values of this ratio and compared with the experimental ones.

The Ce $L_{III}$ threshold XANES spectra of $Ce(acetate)_3$ and $Ce^{3+}$-doped YAG as $Ce^{3+}$ trivalent reference (characteristic peak at 5727 eV) and $CeO_2$ as $Ce^{4+}$ tetravalent reference (characteristic peak at 5738 eV) are shown in **Figure 5.** These two lines are enough dispersed to characterize each oxydation state. The XANES experimental data can be seen also for 0.5% $Ce^{3+}$-doped YAG, 0.5% $Ce^{3+}$-doped GAGG and 0.5% $Ce^{3+}$,0.5% $Mg^{2+}$-co-doped GAGG garnet single-crystals in **Figure 6**, **Figure 7** and **Figure 8,** respectively. It is clear that we do not observe any signal from $Ce^{4+}$ reference in 0.5% $Ce^{3+}$-doped YAG and 0.5% $Ce^{3+}$-doped GAGG and then, only the presence of $Ce^{3+}$ ions is detected in these crystals without any $Mg^{2+}$, whereas in $Ce^{3+}$, $Mg^{2+}$-co-doped GAGG, $Ce^{4+}$ ions are clearly observed. The estimation of the $Ce^{3+}/Ce^{4+}$ ratio in the spectra of 80/20 is the result of the linear combination fit method of the two $Ce^{4+}$ and $Ce^{3+}$ references. In **Figure 7** and **Figure 8,** we choose to drawn the simulation of $Ce^{4+}$ concentration dependences in order to show, at a glance, the evolution of the XANES spectra. The $Ce^{3+}/Ce^{4+}$ ratio of 82.5/17.5 mentionned in **Figure 8** for $Ce^{3+}$, $Mg^{2+}$-co-doped GAGG garnet single-crystal confirms the role of stable $Ce^{4+}$ in the scintillation process and obviously the absence of stable $Ce^{4+}$ in the crystals without any $Mg^{2+}$, as expected. Then, the two methods give the same order of magnitude of the $Ce^{3+}/Ce^{4+}$ ratio value, by considering an error of roughly 10% on the $Ce^{4+}$ value.

Accepted Article

This article is protected by copyright. All rights reserved

It is worth mentioning an absolute quantitative estimation with XANES needs to know the absorption cross sections for both, the $Ce^{3+}$ and $Ce^{4+}$ transitions. If the 4f→5d electric dipole allowed transition cross section is known as high in different materials, the $Ce^{4+}$ charge transfer absorption band is not known. However, a roughly comparison can be done from Figure 2 in $Ce^{3+}$, $Mg^{2+}$-co-doped GAGG garnet single-crystal when comparing the absorption areas of the first $Ce^{3+}$ 4f→5d absorption band at 450 nm with the $Ce^{4+}$ charge transfer absorption band in the 225-325 nm UV spectral range after deducing both $Gd^{3+}$ absorption lines and the second $Ce^{3+}$ 4f→5d absorption band at 340 nm. At a glance, areas shows values of the same order of magnitude giving some sense at the $Ce^{3+}/Ce^{4+}$ ratio deduced from XANES spectra. In $Ce^{3+}$, $Mg^{2+}$-co-doped LYSO and $Ce^{3+}$, $Ca^{2+}$-co-doped LYSO[7], the linear combination fit has been applied and provided 80/20 and 65/35 ratios, respectively, so that, with $Mg^{2+}$ co-doping the same amounts of $Ce^{4+}$ are observed in GAGG and LYSO. In 0.3%$Ce^{3+}$, 0,3%$Mg^{2+}$-co-doped LuAG transparent ceramics the $Ce^{3+}/Ce^{4+}$ ratio is 75/25.[26] The behaviour of $Ce^{3+}$, $Ca^{2+}$-co-doped GAGG garnet single crystal is completely different since the evaluated $Ce^{3+}/Ce^{4+}$ ratio is 4/96. [18]

The segregation coefficient of $Ce^{3+}$ ions in garnets is far from one as we already analyzed it in melt crystal growth and ceramic processing for optical applications in YAG [33-34] and $(Gd,Y)_3Al_5O_{12}$.[35] Here, we started from the nominal concentrations of 1mol.% $Ce^{3+}$, 0.1 mol.% $Mg^{2+}$-co-doped GAGG. and we need to give some values of the real concentrations in the crystals. The solidification fraction (g) described as :g = (mass of grown crystal)/(mass of starting materials in crucible) has been measured and was about 0.23. The composition distributions in grown crystals were monitored by the EPMA; JXA-8621MX, JEOL. The average effective segregation coefficient of $Ce^{3+}$ is $K_{eff}$ = 0.23. As a result, the real concentration of $Ce^{3+}$ in the crystal is estimated between 0.15 and 0.38 mol.%.[16] Traces of $Mg^{2+}$ could not be detected by the EPMA but were analyzed by ICP-AES. $Mg^{2+}$ concentration at g = 0.1 and g = 0.2 were 16 and 25 wt. ppm (0.061 and 0.091 mol%), respectively.

Indeed, we have always to take into account of the competition for scintillation mechanisms between the creation of $Ce^{4+}$ and the presence of the shallow electron traps and deeper traps in the crystal lattice of garnet. These traps capture electrons from the conduction band and contribute to extend component in scintillation decay. It is difficult at this point to evaluate each contribution of $Ce^{4+}$ ion and traps to the fastest component of scintillation response. It is only clear that $Ce^{3+}$, $Mg^{2+}$-co-doped GAGG shows lower afterglow and

Accepted Article

This article is protected by copyright. All rights reserved

thermo-stimulated luminescence intensity[22] and there is an improvement of fast performances from the creation of $Ce^{4+}$. [20]

## 5. XANES data with $Ce^{3+}$-doped LuAG, $Ce^{3+}$, $Li^{+}$-co-doped LuAG and $Ce^{3+}$, $Mg^{2+}$-co-doped LuAG

$Ce^{3+}$-activated LuAG single-crystal is another extensively studied fast and bright scintillator which is demanded in coming medical and industrial applications. Especially, the development of $Ce^{3+}$-doped $Lu_3Al_5O_{12}$ (LuAG)-based single crystal scintillators is a good example of materials prepared by the micro-pulling down method at the initial stage of material screening and by Czochralski or Bridgman methods to obtain higher quality and larger size single crystals afterward.[23] It has been observed that these materials gave rise to new class of ultra-efficient complex oxide scintillators, the light yield of which considerably exceeds the values achieved for the best $Ce^{3+}$-doped orthosilicate scintillators. The interpretation is rather based on trapping processes including the nature and role of material defects giving rise to shallow traps at small energies below the conduction band and $Ce^{4+}$ is not refered. Then, the $Ce^{3+}$, $Li^{+}$ co-doped $Lu_3Al_5O_{12}$ single crystals were also prepared by micro pulling down method and, namely the scintillation decay and light yield have revealed the effect of the co-doping like the smooth $Ce^{4+}$ charge transfer absorption below 350 nm which is clearly enhanced with increasing concentration of $Li^{+}$.[24] Again, the scintillation decays were accelerated and light yields were increased by $Li^{+}$ co-doping. In $Ce^{3+}$, $Ca^{2+}$/$Mg^{2+}$/$Li^{+}$-co-doped LuAG crystals and ceramics, interesting similarities have been found with the previous analysis of $Ce^{3+}$, $Ca^{2+}$/$Mg^{2+}$-co-doped GAGG, mainly by the role demonstrated of $Ce^{4+}$ ions.[25-27] Consequently, it is worthwhile finding out what makes these materials unique and what they all have in common.

Single crystals have been grown also at IMR, Tohoku Unversity, and co-doped not only with $Mg^{2+}$ but also with $Li^{+}$ ions, with the objective to compare results to those of the above GAGG crystals. As for segregation phenomenon, measurements have been done only for $Ce^{3+}$, $Li^{+}$-co-doped GAGG but not for $Ce^{3+}$, $Li^{+}$-co-doped LuAG. From the nominal concentration 0.15mol.% $Li^{+}$,1mol.% $Ce^{3+}$ -co-doped GAGG we have found the average effective segregation coefficient $K_{eff}$ of $Ce^{3+}$, $Ga^{3+}$ and $Al^{3+}$ ions showed $K_{eff}$ = 0.28, 0.94 and 1.06 values respectively. The composition distributions in grown crystals were monitored by the EPMA. Trace of Li could not be detected by the EPMA. Li concentration was analyzed by the glow discharge mass spectrometry (GD-MS). Li concentration at g = 0.1 and g = 0.25

This article is protected by copyright. All rights reserved

Accepted Article

were 5.1 and 3.2 wt ppm (0.023 and 0.014 mol%), respectively. Li concentration was decreased with increasing solidification fraction. This indicates evaporation of Li oxide during the crystal growth. Then, the real composition was 0.023-0.014mol.% $Li^{+}$, Ce 0.25-0.5 mol.% $Ce^{3+}$-co-doped GAGG. We can only say that the real concentration with respect of the nominal concentration in LuAG may vary in the same way as for GAGG due to the same conditions of crystal growths.

The Ce $L_{III}$ -edge XANES spectra of 0.5% $Ce^{3+}$-doped LuAG, 0.5% $Ce^{3+}$,0.5% $Li^{+}$- co-doped LuAG and 0.5% $Ce^{3+}$, 0.3% $Mg^{2+}$-co-doped LuAG shown in **Figure 9** are the first spectra ever recorded for these crystals. First, we note it make sense that $Ce^{3+}$-doped LuAG does not contain any trace of $Ce^{4+}$, as well non-co-doped $Ce^{3+}$-doped YAG and $Ce^{3+}$-doped GAGG. Only $Ce^{3+}$, $Mg^{2+}$-co-doped LuAG shows a weak noisy signal at 5738 eV and then shows the presence of traces of $Ce^{4+}$ ion consistently with $Ce^{3+}$, $Mg^{2+}$-co-doped GAGG. To confirm this $Ce^{4+}$ signal, let's remind Nikl & al[19] have reported the $Ce^{4+}$ charge transfer absorption band clearly observed and enhanced with increasing concentration of $Mg^{2+}$ codopant. We have also compared the XANES spectrum with the weak XANES spectra analysed in $Ce^{3+}$, $Mg^{2+}$-co-doped LuAG transparent ceramic[26]. It makes sense to compare the results of both, crystal (0.5% $Mg^{2+}$) and transparent ceramics (0.3% $Mg^{2+}$ corresponding to the maximum of light output at 25070 ph/MeV). The $Ce^{4+}$ concentration of 25% has been evaluated in this transparent ceramics and clearly increased to 37% of $Ce^{4+}$ ion when the $Mg^{2+}$ concentration was increased from 0.3% to 0.6%. As a result, we can conclude that $Ce^{4+}$ ion plays the same role with the same concentrations in scintillation mechanisms of $Ce^{3+}$, $Mg^{2+}$-co-doped LuAG garnet, either for crystal or for transparent ceramics.

On the other hand, a major feature has to be mentioned: XANES spectra does not show any trace of $Ce^{4+}$ in $Ce^{3+}$, $Li^{+}$-co-doped LuAG. It means, although interesting scintillation data have been reported, the real role of $Ce^{4+}$ remains questionable[23–24]. As an example, an increase of the absorption below 350 nm that could be related to formation of $Ce^{4+}$ oxidation state has been recorded in $Ce^{3+}$, $Li^{+}$-co-doped LuAG grown by micro-pulling and compared to $Ce^{3+}$-doped LuAG, the scintillation decay was accelerated and the high light yield of 24,000 photon/MeV was obtained with 0.2% Li (200 ppm) co-doped samples.[31] It has been suggested that $Li^{+}$ ions in $Ce^{3+}$, $Li^{+}$-co-doped LuAG do substitute $Lu^{3+}$ sites with charge balance attained in part by conversion of $Ce^{3+}$ to $Ce^{4+}$ and creation of O− hole centers, whereas in $Ce^{3+}$, $Li^{+}$-co-doped YAG, $Li^{+}$ goes in interstitial position with charge compensation attained by reduction of anion vacancies.[22,29] The behaviour of these Lu-based

This article is protected by copyright. All rights reserved

garnet scintillators is then different from other Y or Gd-based garnets and should be more deeply analysed. The absence of detectable $Ce^{4+}$ ion from these XANES spectra, as compared with those of $Ce^{3+}$, $Mg^{2+}$-co-doped GAGG and $Ce^{3+}$, $Mg^{2+}$-co-doped LuAG, induces some questions on the scintillation mechanism in $Ce^{3+}$, $Li^{+}$- co-doped LuAG.

## 6. Conclusion

In this work, we were dealing with the most advanced oxide scintillator $Ce^{3+}$, $Mg^{2+}$-co-doped $Gd_3Al_2Ga_3O_{12}$ (GAGG) garnet host, grown at the Tohoku University, Sendai, for applications which require fast timing resolution and high light yield such as PET. The co-doping of $Ce^{3+}$ ion by $Mg^{2+}$ one has revealed the creation of $Ce^{4+}$ ion, assigned from the charge transfer absorption band in UV, due to charge compensation effect, occuring in the scintillation mechanisms, in addition of the usual $Ce^{3+}$ ion, like in $Ce^{3+}$, $Ca^{2+}$-co-doped GAGG and $Ce^{3+}$, $Mg^{2+}$-co-doped LYSO oxydes. The presence and then the role played by the stable $Ce^{4+}$ ion in this garnet for the scintillation mechanisms has been demonstrated by XANES spectroscopy at the Ce $L_{III}$ threshold of the European Synchrotron Radiation Facility (ESRF) in Grenoble. In addition, the estimation of the $Ce^{3+}/Ce^{4+}$ ratio measured by a linear combination fit method is 80/20 and 82.5/17.5 from the simulation of $Ce^{4+}$ curves.

XANES analysis also reveals the creation of $Ce^{4+}$ in $Ce^{3+}$, $Mg^{2+}$-co-doped LuAG crystal, another important scintillator, like it was shown in transparent ceramics of the same composition and confirms the absence of stable $Ce^{4+}$ in crystals like $Ce^{3+}$-doped GAGG, $Ce^{3+}$-doped LuAG and $Ce^{3+}$-doped YAG, respectively, without any $Mg^{2+}$ ion. It means that the scintillation mechanisms are probably the same in $Ce^{3+}$, $Mg^{2+}$-co-doped GAGG and $Ce^{3+}$, $Mg^{2+}$-co-doped LuAG garnet crystals with the occurrence of stable $Ce^{4+}$ ion. On the other side, any trace of $Ce^{4+}$ ion has not been detected in $Ce^{3+}$, $Li^{+}$-co-doped LuAG, in which $Mg^{2+}$ has been substituted by $Li^{+}$. Nevertheless, this crystal is considered as efficient for scintillation. Despite some discussion in literature on the nature of luminescence centers, the real mechanisms of scintillation with $Li^{+}$ ions have to be more clearly understood.

**References**

[1] M. Balcerzyk, Z. Gontarz, M. Moszyski, M. Kapusta, *J. Lumin.* **2000**, *87*, 963.

[2] M. Conti, *Phys. Med.* **2009**, *25*, 1.

[3] M. Nikl, A.Yoshikawa, *Adv. Opt. Mater.* **2015**, *3(4)*, 463.

[4] C. L. Melcher and J. S. Schweitzer, *IEEE Trans. Nucl. Sci.* **1992**, 39, 502.

[5] M. Kapusta, P. Szupryczynski, C. L. Melcher, M. Moszynski, M. Balcerzyk, and A. A. Carey, *IEEE Trans. Nucl. Sci.* **2005**, *52(4),* 1098.

This article is protected by copyright. All rights reserved

Accepted Article

[6] M. A. Spurrier, P. Szupryczynski, A. A. Carey, and C. L. Melcher, *IEEE Trans. Nucl. Sci.* **2008**, *55(3),* 1178.

[7] S. Blahuta, A. Bessière, B. Viana, P. Dorenbos, and V. Ouspenski, *IEEE Trans. Nucl. Sci.* **2013**, *60*, 3134.

[8] K. S. Shah, J. Glodo, M. Klugerman, W. W. Moses, S. E. Derenzo, and M. J.Weber, *IEEE Trans. Nucl. Sci.* **2003**, *50(6),* 2410.

[9] K. W. Kramer, P. Dorenbos, H. U. Gudel, and C. W. E. van Eijk, *J. Mater. Chem.* **2006**, *16*, 2773.

[10] M. S. Alekhin, *Appl. Phys. Lett.* **2014**, *104*, 161915.

[11] K. Kamada, T. Yanagida, J. Pejchal, M. Nikl, T.Endo, K. Tsutumi, Y. Fujimoto, A. Fukabori and A. Yoshikawa, *J. Phys. D: Appl. Phys*. **2011**, *44(50),* 505104.

[12] K. Kamada, T. Endo, K. Tsutumi, T. Yanagida, Y. Fujimoto, A. Fukabori, Y.Yoshikawa, *Cryst. Growth Des.* **2011**, *11*, 4484.

[13] K. Kamada, T. Yanagida, T. Endo, K. Tsutumi, Y. Usuki, and M. Nikl, *J. Cryst. Growth* **2012**, *352*, 88.

[14] M. Tyagi, F. Meng, M. Koschan, S. B. Donnald, H. Rothfuss, C. L. Melcher, *J. Phys. D, Appl. Phys.* **2013**, *46*, 475302.

[15] K. Kamada, S. Kurosawa, P. Prusa, M. Nikl, V. Kochurikhin, T. Endo, K.Tsutumi, H. Sato, Y. Yokota, K. Sugiyama, A. Yoshikawa, *Opt. Mater*. **2014**, *36*, 1942.

[16] K. Kamada, Y. Shoji, V. Kochurikhin, A. Nagura, S. Okumura, S. Yamamoto, J. Yeom, S. Kurosawa, J. Pejchal, Y. Yokota, Y. Ohashi, M. Nikl, M. Yoshino, A. Yoshikawa *IEEE Trans. Nucl. Sci.* **2016,** *63(2),* 443.

[17] J. Yeom, S.Yamamoto, S. E. Derenzo, V. Ch. Spanoudaki, K. Kamada, T. Endo, C. S. Levin, *IEEE Trans. Nucl. Sci* **2013,** *60(2)*, 988.

[18] Y. Wu, F. Meng, Q. Li, M. Koschan, Ch. L. Melcher1, *Phys. Rev. Appl*. **2014**, *2*, 044009.

[19] M. Nikl, K. Kamada, V. Babin, J. Pejchal, K. Pilarova, E. Mihokova, A. Beitlerova, K. Bartosiewicz, S. Kurosawa, and A. Yoshikawa, *Cryst. Growth Des.* **2014,** *14*, 4827.

[20] K. Kamada, M. Nikl , S. Kurosawa, A. Beitlerova, A. Nagura, Y. Shoji, J. Pejchal, Y. Ohashi, Y. Yokota, A. Yoshikawa, *Opt. Mater.* **2015**, *41*, 63.

[21] K. Kamada, Y. Shoji, V. Kochurikhin, A. Nagura, S. Okumura, S. Yamamoto, J. Yeom, S. Kurosawa, J. Pejchal, Y. Yokota, Y. Ohashi, M. Nikl, M. Yoshino, A. Yoshikawa, *IEEE Trans. Nucl. Sci.* **2016**, *63(2)*, 443.

[22] W. Chewpraditkul, N. Pattanaboonmee, O. Sakthong, K. Wantong, W. Chewpraditkul, A. Yoshikawa, K. Kamada, S. Kurosawa, T. Szczesniak, M. Moszynski, V. Babin, M. Nikl,

Accepted Article

This article is protected by copyright. All rights reserved

*Opt. Mater.* **2019**, *92*, 181.

[23] M. Nikl, A.Yoshikawa, K. Kamada, K. Nejezchleb, C.R. Stanek, J.A. Mares, K. Blazek, *Prog. Cryst. Growth Charact. Mater.* **2013**, *59*, 47.

[24] K. Kamada, M. Nikl, S. Kurosawa, A. Beitlerova, A. Nagura, Y. Shoji, J. Pejchal, Y. Ohashi, Y. Yokota and A. Yoshikawa, *J. Cryst. Growth* **2016**, *452*, 85.

[25] S. Liu, X. Feng, Z. Zhou, M. Nikl, Y. Shi, and Y. Pan, *Phys. Status Solidi RRL*, **2014**, *8(1)*, 105.

[26] S. Liu, J. A. Mares, X. Feng, A. Vedda, M. Fasoli, Y. Shi , H. Kou, A. Beitlerova, L. Wu, C. D'Ambrosio, Y. Pan, M. Nikl, *Adv. Opt. Mater.* **2016**, *4*, 731.

[27] J. Li, S. Sahi, M. Groza, Y. Pan, A. Burger, R. Kenarangui, W. Chen, *J. Am. Ceram. Soc.* **2017**, *100*, 150.

[28] S. R. Rotman, H. L. Tuller, and C. Warde, *J. Appl. Phys.* **1992**, *71*, 1209.

[29] M. V. Derdzyan, K. L. Hovhannesyan, A. V. Yeganyan, R. V. Sargsyan, A. Novikov, A. G. Petrosyan, C. Dujardin, *Cryst. Eng. Comm.* **2018**, *20*, 1520.

[30] K. Bartosiewicz, V. Babin, K. Kamada, A. Yoshikawa, M. Nikl, *J. Lum.* **2015,** *166*, 117.

[31] M. Tella, M. Auffan, L. Brousset, E. Morel, O. Proux, C. Chanéac, B. Angeletti, C. Pailles, E. Artells, C. Santaella, J. Rose, A. Thiéry, J.-Y. Bottero, *Environ. Sci.: Nano*, **2015**, *2*, 653.

[32] https://bruceravel.github.io/demeter/

[33] V. Chani, G. Boulon, W. Zhao, T. Yanagida, A.Yoshikawa, *Jpn. J. App. Phys.* **2010**, 49 075601.

[34] W. Zhao, S. Anghel, C. Mancini, D. Amans, G. Boulon, T. Epicier, Y. Shi, X.Q. Feng, Y.B. Pan, V. Chani, A. Yoshikawa, *Opt. Mater.* **2011**, 33, 684–687.

[35] W. Zhao, C. Mancini, D. Amans, G. Boulon, T. Epicier, Y. Min, H. Hideki, T. Yanagitani, T. Yanagida, A. Yoshikawa, *Jpn. J. App. Phys.* **2010**, 49 022602.

Accepted Article

This article is protected by copyright. All rights reserved

FIGURES

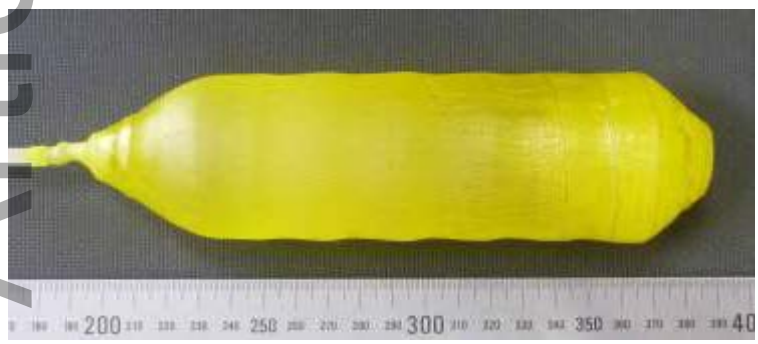

**Figure 1a** Garnet single crystal: 2 inch size 1%$Ce^{3+}$-doped $Gd_3Al_2Ga_3O_{12}$ (GAGG) garnet single crystal grown by the CZ method at IMR, Tohoku University, Sendai, Japan.

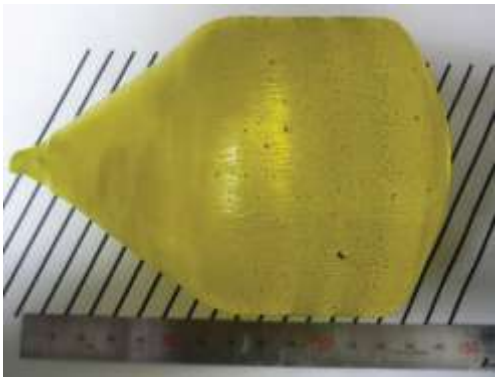

**Figure 1b** Garnet single crystal: 3 inch diameter of 1%Ce, 0.1%Mg-co-doped $Gd_3Al_2Ga_3O_{12}$ (GAGG) garnet single crystal grown by the CZ method at IMR, Tohoku University, Sendai, Japan.

Accepted Article

This article is protected by copyright. All rights reserved

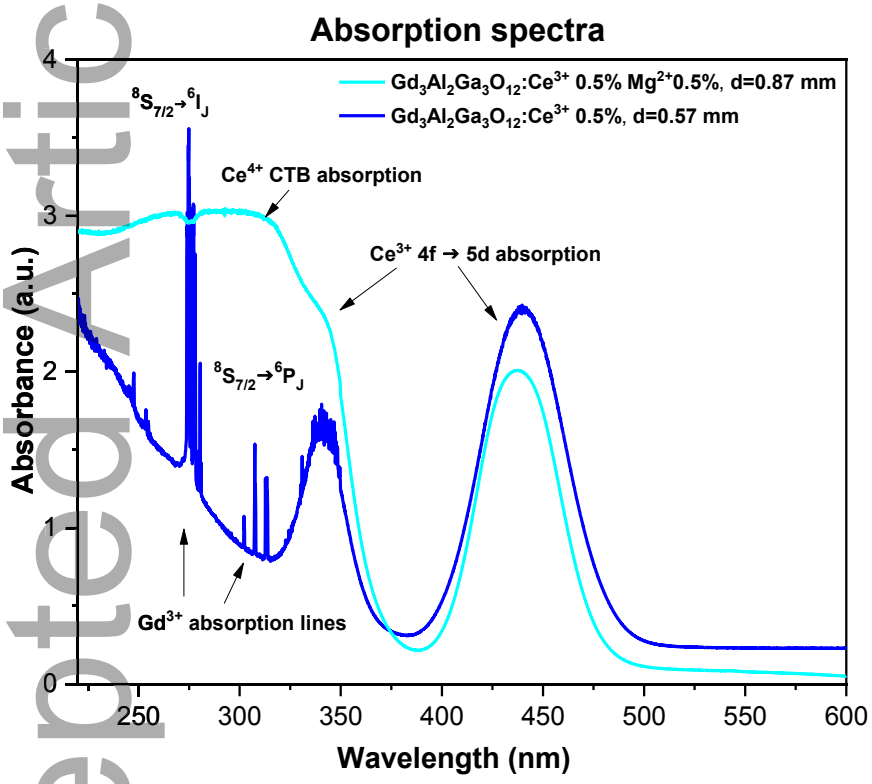


**Figure 2** Absorption spectra at room temperature of the 0.5% $Ce^{3+}$-doped GAGG and 0.5% $Mg^{2+}$, 0.5% $Ce^{3+}$-co-doped GAGG crystals, at room temperature.

Accepted Article

This article is protected by copyright. All rights reserved

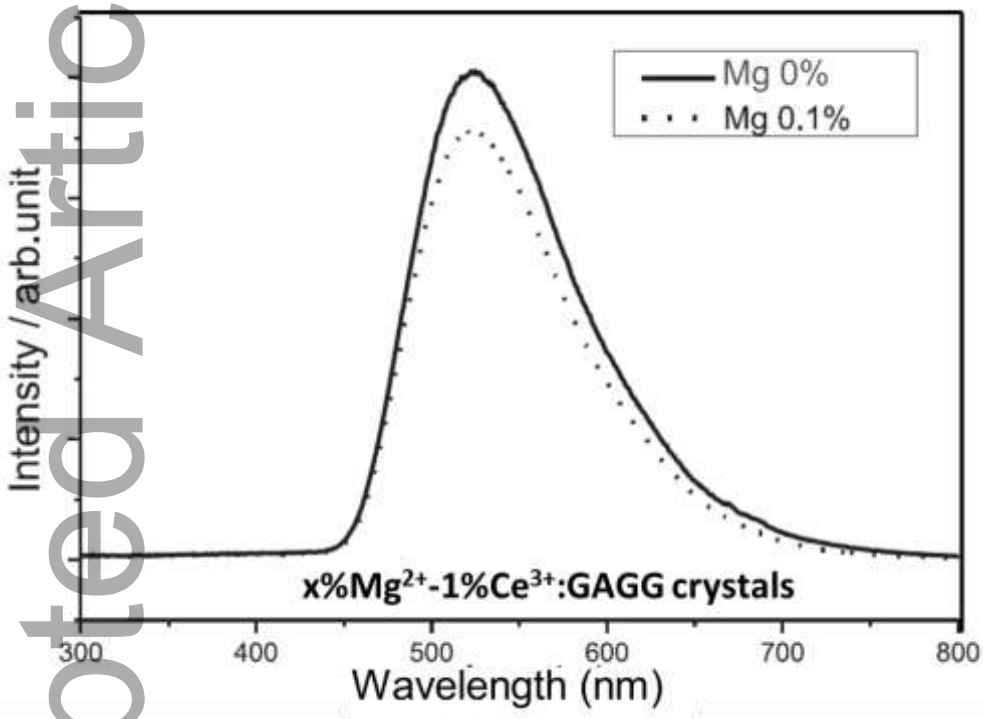


**Figure 3** Radioluminescence spectra at room temperature of the 5d→4f transition of $Ce^{3+}$ in 1% $Ce^{3+}$:GAGG and 0.1% $Mg^{2+}$, 1% $Ce^{3+}$-co-doped GAGG crystals. Excitation by X-rays, CuKa, 40 kV, 30 mA.

Accepted Article

This article is protected by copyright. All rights reserved

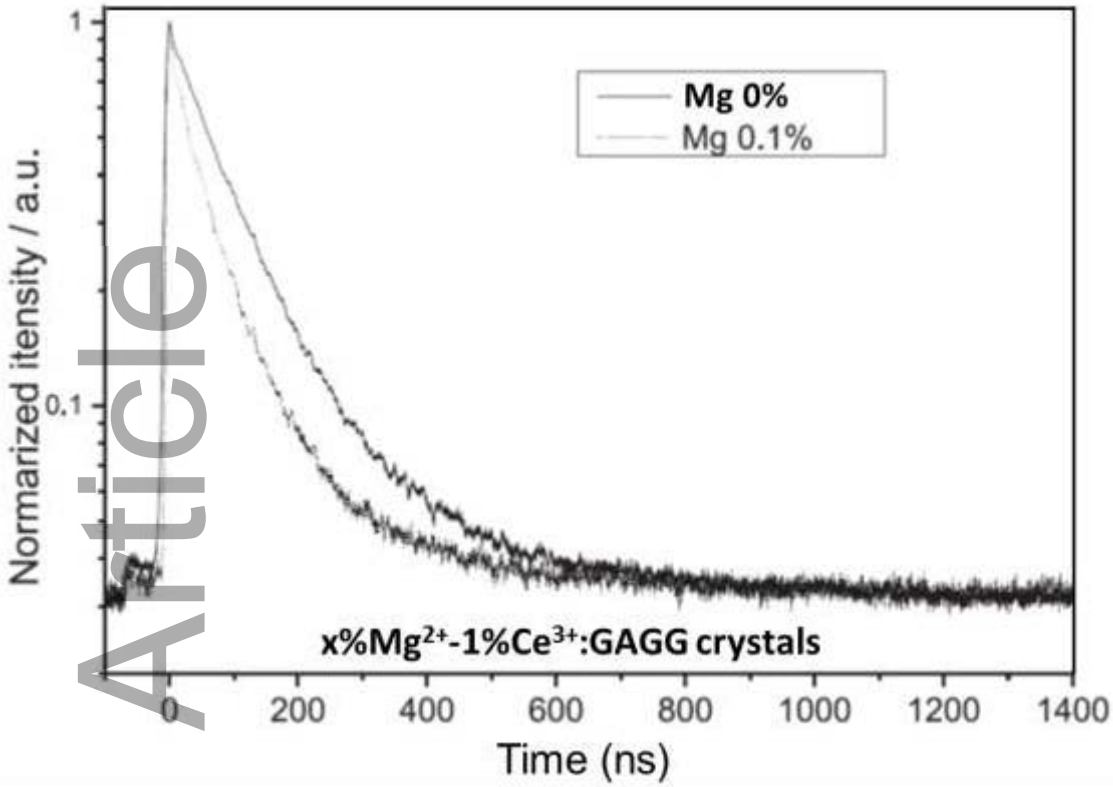


**Figure 4** Scintillation decay profiles at room temperature of the 5d→4f visible broad band of the 1%$Ce^{3+}$-doped GAGG (0% $Mg^{2+}$) and 1%$Ce^{3+}$, 0.1%$Mg^{2+}$-co-doped GAGG crystals under excitation by $^{137}$Cs radio-isotope (662 keV).

Accepted Article

This article is protected by copyright. All rights reserved

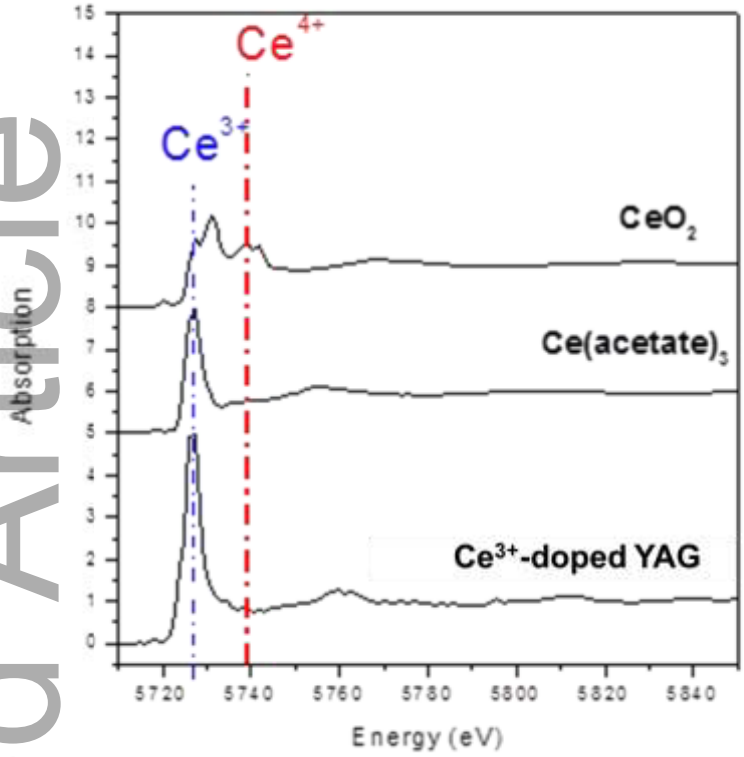


**Figure 5** The XANES spectroscopy at the Ce $L_{III}$ threshold. X-ray absorption spectra of $Ce^{3+}$ and $Ce^{4+}$ are different. $CeO_2$ is chosen as a reference for $Ce^{4+}$ (characteristic peak at 5738 eV) and Ce(acetate)$_3$ and $Ce^{3+}$-doped YAG are chosen as a reference for $Ce^{3+}$ (characteristic peak at 5727 eV).

Accepted Article

This article is protected by copyright. All rights reserved

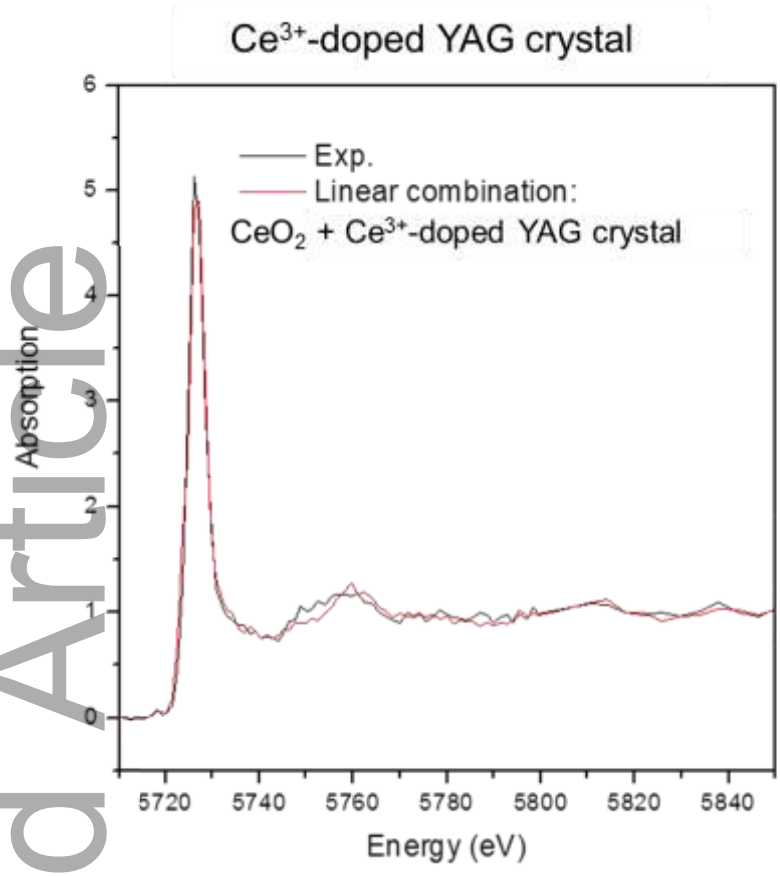


**Figure 6** Comparison of the experimental XANES spectrum of the 0.5% $Ce^{3+}$-doped YAG single-crystal (black, with thickness=0,53mm) with the spectrum obtained by a linear combination fit method. Another $Ce^{3+}$-doped single-crystal is used as a reference for $Ce^{3+}$ (red). We observe the presence of only $Ce^{3+}$ ions in this sample.

Accepted Article

This article is protected by copyright. All rights reserved

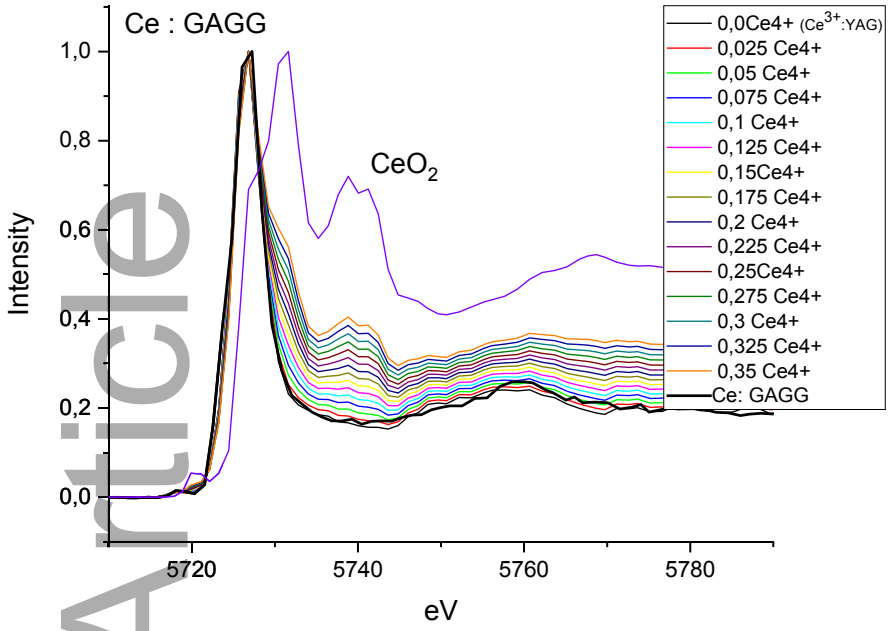


**Figure 7** Experimental Ce $L_{III}$-edge XANES spectra of $Ce^{3+}$-doped GAGG garnet single crystal (black curve). The XANES spectra of the $Ce^{4+}$ ($CeO_2$) and $Ce^{3+}$ ($Ce^{3+}$: YAG) mentioned here by 0.0 $Ce^{4+}$, are used as references. Ratio dependence of XANES spectra have been simulated for different $Ce^{4+}$ concentrations. Any trace of $Ce^{4+}$ has been detected and so the sample contains only $Ce^{3+}$.

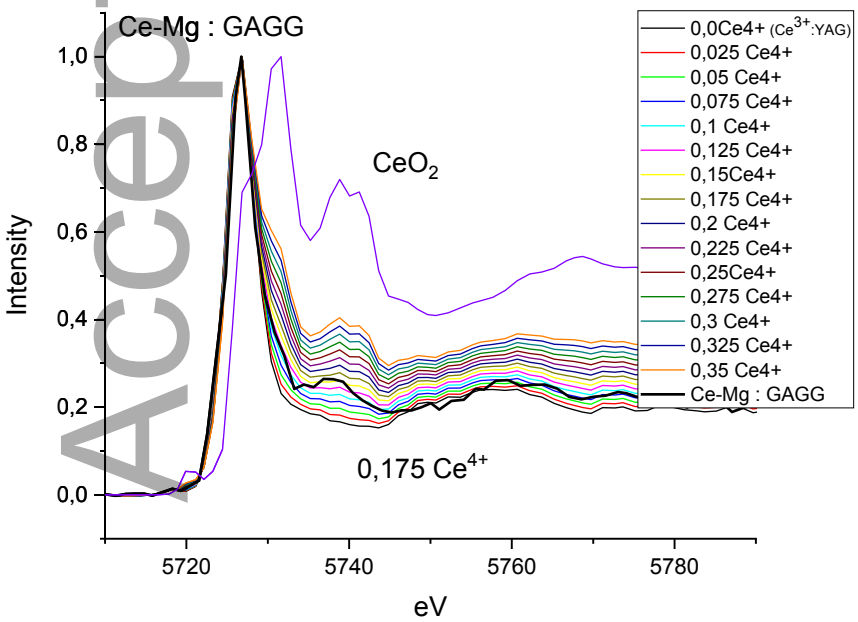


Accepted Article

This article is protected by copyright. All rights reserved

**Figure 8** Experimental Ce $L_{III}$-edge XANES spectra of $Ce^{3+}$, $Mg^{2+}$-co-doped GAGG garnet single crystal (black curve). The XANES spectra of the $Ce^{4+}$ ($CeO_2$) (violet) and $Ce^{3+}$ ($Ce^{3+}$:YAG) mentioned here by 0.0 $Ce^{4+}$ (black), are used as references. Ratio dependence of XANES spectra have been simulated for different $Ce^{4+}$ concentrations. The sample contains 17.5% $Ce^{4+}$ and then 82.5% $Ce^{3+}$.

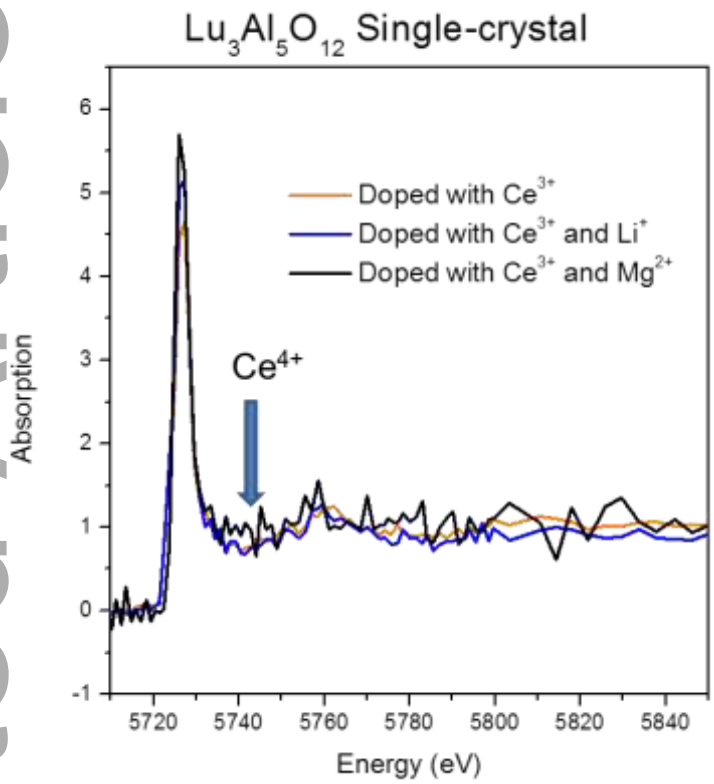


**Figure 9** Experimental Ce $L_{III}$-edge XANES spectra of $Ce^{3+}$-doped LuAG (red), $Ce^{3+}$, $Li^{+}$-co-doped LuAG (blue) and $Ce^{3+}$,$Mg^{2+}$-co-doped LuAG (black), respectively. Only $Ce^{3+}$, $Mg^{2+}$-co-doped LuAG shows a weak noisy signal at 5738 eV and then the presence of $Ce^{4+}$ ion. Thickness of samples=0,53mm.

Accepted Article

This article is protected by copyright. All rights reserved

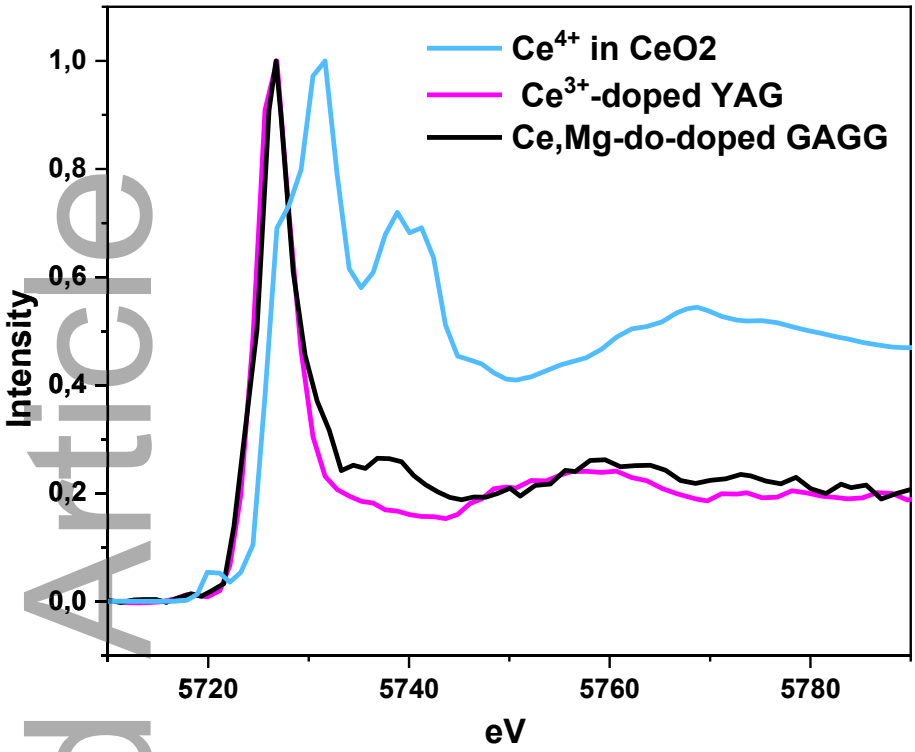


Normalized experimental Ce $L_{III}$-edge XANES spectra of 1%$Ce^{3+}$, 0.1%$Mg^{2+}$-co-doped GAGG garnet single crystal (black curve). The normalized XANES spectra of the $Ce^{4+}$ ion in $CeO_2$ (blue curve) and $Ce^{3+}$-doped YAG (pink curve) are used as references. 0.175%$Ce^{4+}$ and 0.825% $Ce^{3+}$ have been detected.

Accepted Article

This article is protected by copyright. All rights reserved